npj | climate and atmospheric science

www.nature.com/npjclimatsci

ARTICLE OPEN

Check for updates

To what extent can the ozone valley over the Tibetan Plateau influence the East Asian summer precipitation?

Lingaona Zhu[1] and Zhiwei Wu[1]✉

The ozone valley over the Tibetan Plateau (OVTP) has experienced significant interannual variations during the past decades. Previous studies have primarily focused on the origins of OVTP rather than its climate impact. This study reveals that OVTP during its peak season (May–July) explains up to 15% of the summer precipitation variability in East Asia. The results suggest that the surface temperature (T_s) anomaly over the Tibetan Plateau (TP) acts as a link between OVTP and East Asian precipitation. Through the positive land-atmosphere feedback, the T_s anomaly over the TP is amplified. The anomalous T_s pattern persists into summer (June–August) due to the land memory effect and impacts the East Asian precipitation by modulating the local circulation. The Specified-Chemistry version of the Whole Atmosphere Community Climate Model is employed to validate that MJJ OVTP results in a substantial increase of T_s over TP and induces an anomalous anti-cyclone centered over the Yangtze-Huaihe River Basin during summer. Consequently, negative precipitation anomalies are observed in the Yangtze River Basin, while positive precipitation anomalies occur in Southern China. The linear baroclinic model further demonstrates that the diabatic heating over the TP serves as the link between MJJ OVTP and East Asian summer precipitation patterns. Our analysis of Coupled Model Intercomparison Project Phase 6 models reveals that a more accurate prediction of East Asian precipitation requires an improved understanding of the relationship between OVTP and TP T_s.

npj Climate and Atmospheric Science (2023)6:177 ; https://doi.org/10.1038/s41612-023-00508-x

INTRODUCTION

Ozone layer not only provides local heating in the stratosphere but also absorbs ultraviolet radiation to protect the Earth[1]. Therefore, ozone depletion could modulate the global radiative balancing and affect tropospheric climate[2]. Since then, several ozone depletions have been discovered and studied, including the ozone holes over the Antarctic and the Arctic[3–17], as well as the ozone valley over the Tibetan Plateau (OVTP)[18–20].

Previous studies have suggested that the depletion of polar stratospheric ozone has been responsible for most tropospheric circulation changes in the Southern Hemisphere during the austral summer over the second half of the twentieth century[3]. Antarctic ozone depletion leads to cooling and intensification of the polar vortex, along with a poleward shift of the mid-latitude jet stream[3–7]. This process enhances the positive phase of the Southern Hemisphere annular mode and expands the Hadley cell, consequently impacting surface temperature (T_s) and subtropical precipitation in the Southern Hemisphere during the austral summer[3,8]. Although the ozone depletion in the Arctic region has been less pronounced compared to the Antarctic region in the past 30 years, it is still associated with the strengthening of the polar vortex and a notable and persistent shift in the tropospheric circulation towards a positive phase of the Northern Annular Mode[9–11]. Consequently, positive temperature anomalies are observed at the surface in Northern Europe and Siberia, while negative temperature anomalies are observed in China, Greenland, and northeastern Canada[11]. Furthermore, polar ozone depletion also exerts a substantial influence on polar sea ice[12–17], with certain effects attributed to cloud radiative processes[14,17]. These results emphasize the essential impact of ozone depletion in polar regions.

Ozone depletion is not exclusive to polar regions but also occurs in mid-latitude regions. As early as 1995, a notable total column ozone (TCO) depletion center was discovered over the TP in summer using the Total Ozone Mapping Spectrometer satellite data[18]. Subsequent research confirmed the existence of the OVTP based on the analysis of ozone-sounding data collected in Lhasa from June to October 1998[19]. Furthermore, the OVTP was observed to exhibit a double core structure, with a stronger center in the upper troposphere-lower stratosphere (UTLS) region and a weaker center in the upper stratosphere[20]. Since the discovery of OVTP, numerous studies have been dedicated to identifying the factors responsible for its formation[21–34]. Some studies emphasized the role of chemical processes in driving the ozone depletion over the TP[21–23], while others claimed that the influence of the topography of the TP was more crucial than the chemical effect[24–28]. Noticeably, the dominant causes of OVTP formation, according to most studies, are associated with dynamic effects. During summertime, the TP exerts a substantial thermal and dynamic influence on the surrounding atmospheric circulation[18]. As a result, the air in the lower troposphere, which contains lower ozone content compared to the stratosphere, is efficiently transported upward, resulting in a reduction in ozone concentrations at higher altitudes over the region as well as in the TCO. Additionally, the process of stratosphere–troposphere mass exchange[23,29,30], variations in atmospheric circulation associated with the Asian summer monsoon[31–33], and the uplift of isentropic surfaces and tropopause height[24,34] are also recognized as vital contributors to the formation of the OVTP.

Being one of the prominent ozone depletion centers in the world, however, the climate impact of the OVTP has received limited attention in previous studies[31,35–37]. Interactions between the intensity of the South Asia High (SAH) and ozone in

[1]Department of Atmospheric and Oceanic Sciences, Institute of Atmospheric Sciences, and Shanghai Scientific Frontier Base of Ocean–Atmosphere Interaction, Fudan University, 200438 Shanghai, China. ✉email: zhiweiwu@fudan.edu.cn

neighboring regions during summertime have been indicated in several studies[35,36]. Li et al. (2017) suggested that the latitudinal asymmetry of ozone in the UTLS region could induce a latitudinal asymmetry in radiative forcing within the South Asian high-pressure system, which in turn had the potential to affect the South Asian High. Additionally, previous research has shown a close correlation between the variation of total ozone over the TP and the temperature and precipitation patterns in China[37], while the corresponding physical mechanisms still require further investigation and validation. Therefore, it is meaningful to investigate the extent to which the OVTP can influence East Asian summer precipitation and elucidate the corresponding physical mechanism. Zhou and Zhang (2005) suggested, based on observation data, that the OVTP may contribute to the cooling in the stratosphere and warming in the troposphere over the TP in recent decades[31]. Considering the substantial impact of the thermal anomalies over the TP on the East Asian climate[38–42], it is worthwhile to investigate whether the OVTP can influence East Asian precipitation by modifying the thermal anomalies of the TP. In this study, we discover the considerable impact of the May-July (MJJ) OVTP on the East Asian summer precipitation and illustrate the corresponding physical mechanisms. The structure of the paper is organized as follows. Section "Results" describes the relationship between OVTP and East Asian summer precipitation. The impact of the MJJ OVTP on the summer TP thermal anomaly is evaluated in the section "Discussion". Section "Methods" presents the results of numerical experiments assessing the climate impacts of OVTP, along with an examination of the linear response of circulation anomalies over East Asia to TP diabatic heating anomalies.

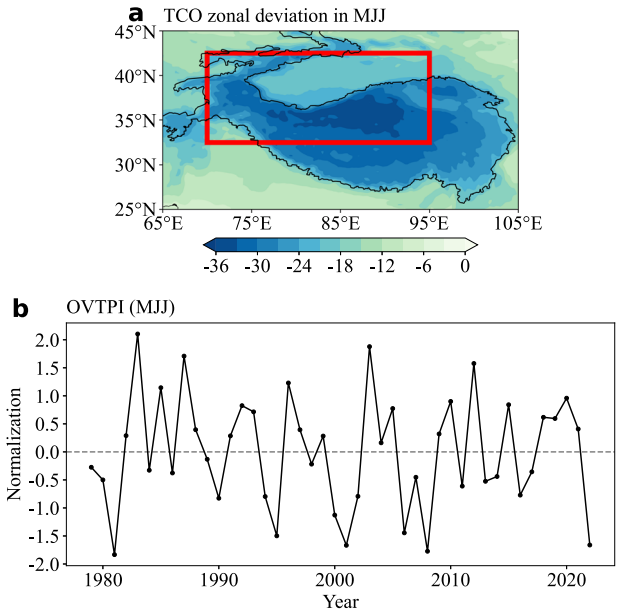

Fig. 1 TCO zonal deviation in MJJ and time series of OVTPI. **a** Long-term mean zonal deviation of the total column ozone (TCO) over the Tibetan Plateau during previous summer (May–June–July, MJJ) for the period 1979–2022. **b** Time series of the normalized OVTPI defined by the inverse zonal deviation of the TCO averaged in the red-boxed area (70°–95°E, 32.5°–42.5°N) in (**a**) during MJJ.

RESULTS

Relationship between the OVTP and the East Asian summer precipitation

To characterize the OVTP, the monthly zonal ozone deviation obtained by subtracting the zonal mean from the TCO is calculated over the Tibetan region (75°–105°E, 25°–45°N)[34,43,44]. The results indicate that the strongest zonal ozone deviation period over the TP occurs from May to July during 1979–2022, dropping below −20 DU (Supplementary Fig. 1). Therefore, we investigate the climate effects induced by the OVTP during these three months. Based on the spatial distribution of the OVTP climatology over the past 44 May–July (MJJ) periods (Fig. 1a), the strongest ozone valley is located over the north-western TP, reaching around −36 DU. To quantitatively measure the interannual variations of the MJJ OVTP, the OVTP index OVTPI is defined as the inverse TCO zonal deviation averaged within the red-boxed area (70°–95°E, 32.5°–42.5°N) in Fig. 1a. Specifically, a higher OVTPI value indicates a stronger OVTP. Consistent with the results in the earlier studies[34,43,44], the time series of the MJJ OVTPI (Fig. 1b) exhibits an interannual variability with no significant trend.

To illustrate the association between OVTPI and East Asian summer precipitation, the regression of East Asian summer precipitation anomalies against the MJJ OVTPI is plotted in Fig. 2. Corresponding to the strengthening of the MJJ OVTP, the precipitation distribution shows a north–south dipole pattern, characterized by negative precipitation anomalies along the Yangtze River Basin to Southern Japan while positive precipitation anomalies in the Indochina Peninsula and Southern China region. The MJJ OVTPI explains about 6–20% of the total variance of the local JJA precipitation along the Yangtze River Basin to Southern Japan, and accounts for approximately 6–12% of the total variance of the local JJA precipitation in the Indochina Peninsula and Southern China region (Fig. 2b).

To further explain the observed precipitation pattern, the geopotential height and wind anomalies at different pressure levels (200, 500, and 850 hPa) regressed against the OVTPI are

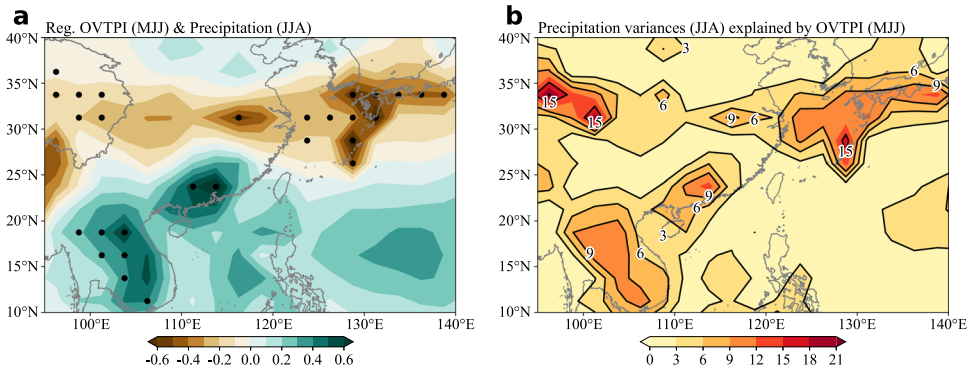

Fig. 2 Precipitation anomalies in JJA associated with MJJ OVTP. **a** JJA precipitation anomalies regressed against the MJJ OVTPI (color shadings; in unit of mm day^{-1}). The dotted areas exceed the 95% confidence level. **b** The JJA precipitation fractional variances explained by the MJJ OVTPI (color shadings; in unit of %).

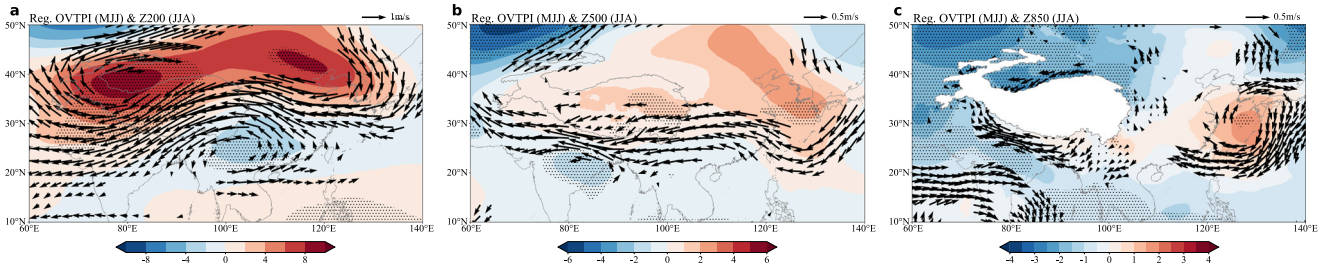

Fig. 3 Relationship between MJJ OVTP and atmospheric circulation anomalies in JJA. JJA geopotential height anomalies (shading, unit: gpm) and wind anomalies (vector, unit: m s^{-1}) regressed against the MJJ OVTPI at **a** 200, **b** 500, **c** 850 hPa. The dotted areas and the black vectors exceed the 90 % confidence level.

examined (Fig. 3). At 200 hPa, there is a distinct north-south dipole pattern in geopotential height anomalies. A positive anomaly center is located over north-eastern China, while a negative anomaly center is observed over Southern China. Meanwhile, a positive anomaly center in geopotential height is observed over the northwestern Pacific at 500 hPa. At 850 hPa, high-pressure anomalies are found over the northwestern Pacific, corresponding to negative precipitation anomalies along the Yangtze River Basin to Southern Japan (Fig. 2a). Concurrently, easterly wind anomalies along the southeastern coast of China contribute to the transport of moisture, leading to the observed positive precipitation anomalies in Southern China (Fig. 2a).

Therefore, the question arises: how does the preceding OVTPI influence summer circulation patterns and lead to the observed precipitation anomalies in East Asia? Previous studies have provided evidence that ozone in the UTLS region significantly influences the radiation budget and T_s[31,45–47]. Additionally, the thermal anomaly of the TP has been shown to impact East Asian precipitation[38–42]. Based on the studies above, we have formulated a hypothesis: can the OVTP influence East Asian precipitation by modifying the T_s of the TP? To explore this hypothesis, we first need to investigate the impact of the preceding OVTP on the summer TP thermal anomaly.

Impact of the MJJ OVTP on the JJA TP thermal anomaly

Vertical-latitude cross sections along 70°–95°E in MJJ are depicted in Fig. 4. Corresponding to the intensification of the OVTP, negative ozone anomalies are observed at altitudes ranging from 50 to 200 hPa, with a particularly significant depletion occurring around 150 hPa. Due to the depletion of ozone in the UTLS over the TP, less ultraviolet radiation is absorbed in the lower stratosphere, resulting in an increased amount of radiation reaching the troposphere and the TP surface[31]. As a result, a prominent feature is the occurrence of negative temperature anomalies above 150 hPa, while positive temperature anomalies occur below this height (Fig. 4b). Additionally, cooling in the stratosphere is favorable for air mass descent[31]. The subsidence of cooled air masses above 100 hPa can result in a high-pressure anomaly around 150 hPa. The observed phenomenon and the physical mechanism described here are consistent with the findings of Zhou and Zhang (2005), which suggest that ozone depletion is likely an important external forcing in influencing temperature and general circulation in the TP region. Moreover, the high-pressure anomaly around 150 hPa would lead to a reduction in low cloud cover[48,49] (Fig. 4d), which in turn amplifies the T_s anomaly over TP.

In previous studies, a positive land–atmosphere feedback process involving heat waves, cloud cover, the atmospheric boundary layer, and surface sensible heat flux (ISHF) was proposed[49–51]. To investigate whether there is a positive land–atmosphere feedback process that amplifies the impact of OVTP on T_s over the TP, the regression of MJJ T_s anomalies, boundary layer height (BLH) anomalies, total cloud cover (TCC) anomalies, and ISHF anomalies against the MJJ OVTPI are plotted (Fig. 5). Corresponding to the strengthening of the OVTP, positive T_s anomalies (Fig. 5a) and BLH anomalies (Fig. 5b) are observed, whereas negative TCC anomalies (Fig. 5c) and ISHF anomalies (Fig. 5d) are identified. Negative TCC anomalies are usually associated with increased shortwave radiation and surface sensible heat flux[50,51]. These anomalies lead to a deepening of the atmospheric boundary layer, which in turn contributes to a further reduction in TCC. Based on the results from Supplementary Table 1, OVTPI, T_s, BL, TCC, and ISHF exhibit significant correlations with each other over north-western TP. Consequently, it is evident that the MJJ OVTP exerts a substantial influence on T_s over the TP by amplifying its impact through positive land–atmosphere feedback. This raises the next question: how does the MJJ OVTP affect T_s in the subsequent summer?

Comparing T_s anomaly patterns between the period of MJJ (Fig. 5a) and JJA (Fig. 6a) regressed against MJJ OVTPI, the influence of OVTP on the T_s anomaly pattern persists from MJJ to JJA. The land T_s anomaly in the TP has been observed and supported by model simulations to persist over seasons[52,53]. This sustained anomaly is often accompanied by subsurface temperature, snow cover, and surface albedo anomalies[52]. To explore the potential factors contributing to the persistence in this study, a comparison is made between the persistent component of T_s and JJA T_s anomaly regressed against MJJ OVTPI. According to Pan (2005)[54], the persistent component of the T_s in JJA, T_{sp}, can be calculated as

$$T_{sp} = T_s(\mathrm{MJJ})\mathrm{Cov}[T_s(\mathrm{JJA}), T_s(\mathrm{MJJ})]/\mathrm{Var}[T_s(\mathrm{MJJ})] \quad (1)$$

The terms Cov and Var in Eq. (1) denote covariance and variance, respectively. The dominant pattern of the T_s persistent component (Fig. 6b) exhibits minimal changes in comparison to that of the total T_s (Fig. 6a), as indicated by their high pattern correlation coefficient of approximately 0.88. Therefore, the land memory effect should be considered as a critical factor in sustaining the influence of OVTP on the T_s anomaly pattern from MJJ to JJA.

Numerical experiments

To confirm the impact of OVTP on East Asian climate, we conducted two simulations with different ozone prescriptions in the Specified-Chemistry version of the Whole Atmosphere Community Climate (SC-WACCM) model. In the control experiment, denoted as 'before_remove', monthly mean ozone concentrations from the year 2000 are prescribed, and the model is run for a duration of 25 years. In the sensitivity experiment, referred to as 'after_remove', we implement the removal of the OVTP by replacing the MJJ ozone mixing ratio at each level over the TP region (70°–105° E, 25°–40°N) with zonal mean ozone values. The sensitivity simulation is also run for a 25-year period. We evaluate the effects of the OVTP on East Asian climate by comparing the differences between the last 10-year averages of the 'before_remove' and 'after_remove' simulations.

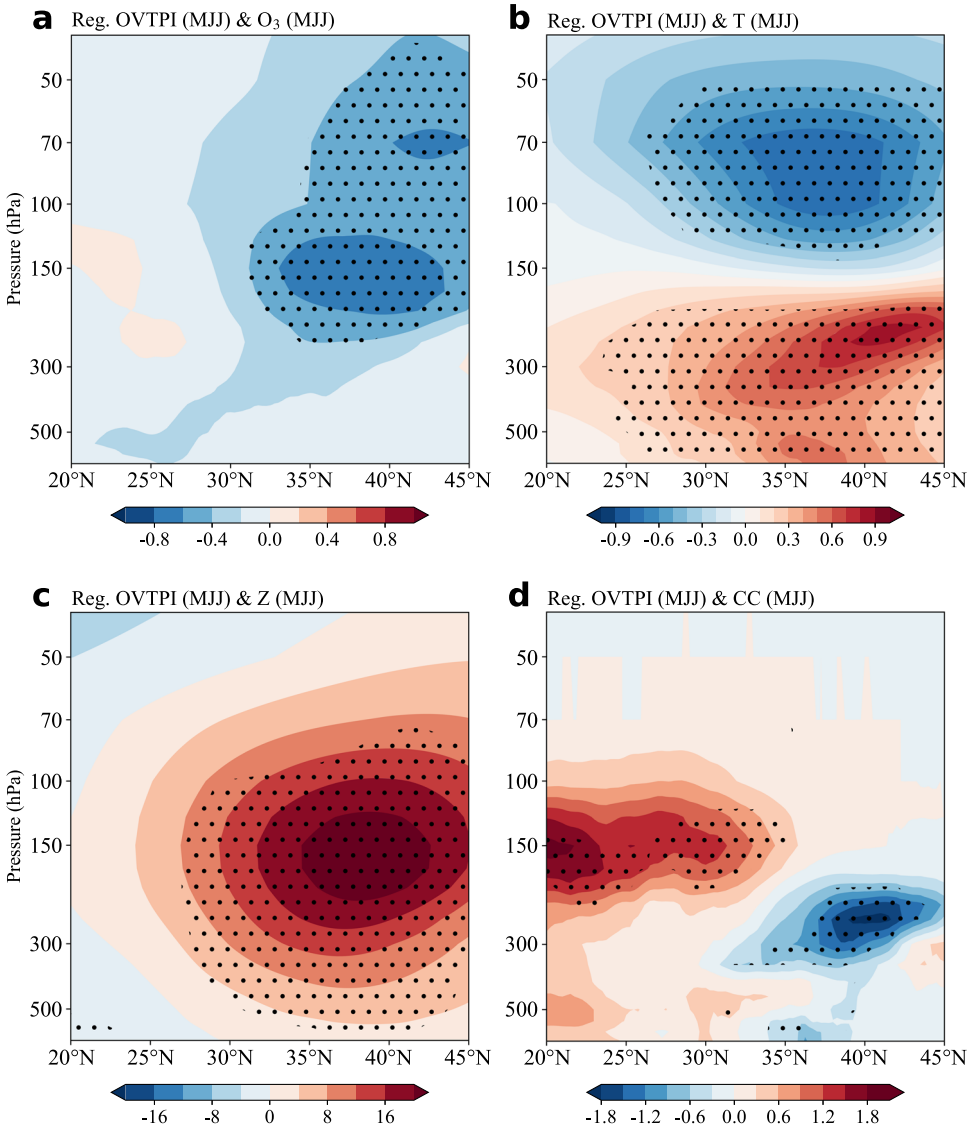

Fig. 4 Relationship between MJJ OVTP and vertical-latitude cross sections of MJJ anomalies. Vertical-latitude cross sections of MJJ **a** TCO anomalies (shading, unit: DU), **b** temperature anomalies (shading, unit: K); **c** geopotential height anomalies (shading, unit: gpm); **d** cloud cover anomalies (shading, unit: %) regressed against the MJJ OVTPI along 70°–95°E. The dotted areas exceed the 95% confidence level.

Figure 7a illustrates the differences in prescribed ozone between the two experiments, while Fig. 7b–d depict the simulated differences in temperature, geopotential height, and cloud cover between two experiments (before_remove−after_remove) along 85–100° E during MJJ. According to the findings, a reduction of approximately 1.2 to 2×10^{-7} mol mol^{-1} in ozone from 50–150 hPa results in a temperature decrease of −0.3 to −0.8 K from 70–150 hPa, while simultaneously leading to an increase of 0.3–0.8 K in the troposphere, extending down to the surface. This effect is particularly prominent between 30°N and 40°N. The temperature increase in the troposphere and at the surface is primarily attributed to the rising net heating rate below 200 hPa, which reaches 1.2×10^{6} K s^{-1} (Fig. 7e). Meanwhile, there is a pronounced increase in geopotential height between 100 and 300 hPa, reaching its peak at 200 hPa. The influence of OVTP on geopotential height reduces cloud cover below 300 hPa (Fig. 7d), thereby triggering the positive land-atmosphere feedback discussed in the previous section and further increasing T_s over the TP. The results from SC-WACCM are consistent with the observations shown in Fig. 4. This demonstrates that the OVTP can indeed exert a substantial influence on T_s and geopotential heights over the TP. The T_s difference between MJJ and JJA in Supplementary Fig. 2 illustrates the sustained influence of OVTP on local T_s from MJJ to JJA. During JJA, the presence of OVTP in MJJ leads to a warming of T_s on the Central-Western region of the TP by 0.3–0.8 K. Overall, these findings confirm that the OVTP during MJJ can intensify the thermal anomaly of the TP during JJA.

To verify whether OVTP affects the East Asian summer circulation and precipitation, Fig. 8 represents the simulated JJA atmospheric circulation anomaly induced by the OVTP. At 200, 500, and 850 hPa, high-pressure anomalies extend from East China through the Yellow Sea to Southern Japan. The high-pressure anomalies in the northwest Pacific are similar with the observed results (Fig. 3), particularly at 500 and 850 hPa, leading to a negative precipitation anomaly that extends from the Yangtze River Basin to Southern Japan. Meanwhile, the anomalous eastward winds on the southern side of the anti-cyclone system transport moisture from the western Pacific, contributing to increased rainfall in Southern China. So far, we have demonstrated that MJJ OVTP can simultaneously impact T_s and East Asian circulation during JJA. However, it has not yet been proven that OVTP influences East Asian circulation through its impact on T_s.

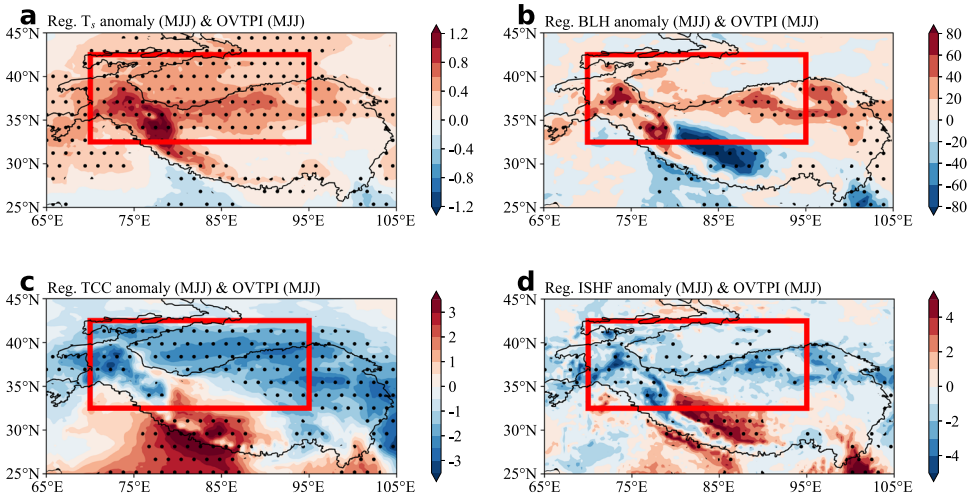

Fig. 5 Physical variables associated with surface–atmosphere coupling over TP. MJJ **a** T_s anomalies (shading, unit: K), **b** boundary layer height (BLH) anomalies (shading, unit: m); **c** total cloud cover (TCC) anomalies (shading, unit: %); **d** instantaneous surface sensible heat flux (ISHF) anomalies (shading, unit: J m^{-2}) regressed against the MJJ OVTPI. The dotted areas exceed the 95% confidence level.

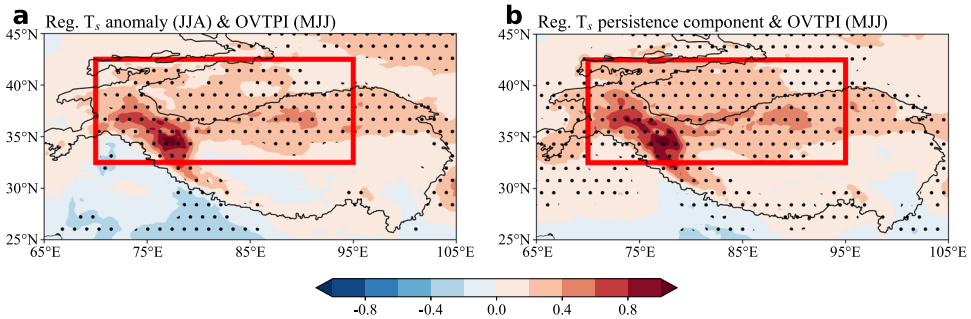

Fig. 6 Persistence of MJJ T_s over TP. JJA **a** T_s anomalies (shading, unit: K) and **b** the persistence component of T_s regressed against MJJ OVTPI. The dotted areas exceed the 95% confidence level.

To further investigate whether the OVTP affects East Asian precipitation through its influence on the thermal anomaly of the TP, we have designed another numerical experiment using the linear baroclinic model (LBM). The thermal forcing is distributed within an elliptical region centered at 77°E, 35°N, with radiuses of 8° and 10° in the latitudinal and longitudinal directions, respectively. An idealized warming profile with a maximum value of 1 K day^{-1} at the 0.75 sigma level (around 400 hPa) is employed to mimic the OVTP-induced diabatic warming effect (Fig. 9). This experiment is performed with a basic state of the summer climatology. The LBM is integrated for 40 days, and the variables during the last 10 days are averaged to obtain the stabilizing state for further analysis.

Figure 9c–e shows the simulated response of the atmospheric circulation over East Asia to the heating forcing over the north-western TP. A positive geopotential height anomaly is induced at the upper troposphere over TP, which extends eastward towards northeastern China (Fig. 9c). Meanwhile, the anti-cyclone system over northeastern China also occurs at 500 hPa (Fig. 9d). At 850 hPa, the center of the anti-cyclone system is located in the Yangtze-Huaihe River Basin, accompanied by easterly winds along the southeast coast of China (Fig. 9e). The anomalous circulation pattern, which is in good agreement with the observed circulation shown in Fig. 3c, plays a crucial role in generating negative precipitation anomalies in the Yangtze River Basin and positive precipitation anomalies in Southern China through the transport of moisture. Overall, the results from LBM demonstrate that the heating forcing over the north-western TP acts as a link between the OVTP and precipitation in East Asia.

DISCUSSION

The depletion of ozone has significant implications for both ecosystems and climate. Previous studies have primarily focused on the causes and climate impacts of polar ozone holes, while the climate impact of the OVTP has received limited attention. In this study, we aim to quantify the contribution of the OVTP during its peak season of MJJ to East Asian summer precipitation. Our findings reveal that the OVTP explains up to 15% of the variability in summer precipitation in East Asia. Moreover, we identify the T_s anomaly over the TP as a crucial link between the OVTP and East Asian precipitation. Numerical experiments confirm that the intensification of MJJ OVTP, characterized by a significant reduction in TCO from 50 to 150 hPa, leads to a notable decrease in stratospheric temperature due to reduced absorption of radiation. This, in turn, allows more radiation to reach the troposphere and surface. Additionally, the intensification of MJJ OVTP also leads to a high-pressure anomaly near 200 hPa. This anomaly suppresses cloud formation near the surface, leading to an increase in local net shortwave radiation and surface sensible heat flux. Consequently, the atmospheric boundary layer rises and further inhibits cloud formation. Through this positive land-atmosphere feedback, the T_s anomaly over the TP is reinforced. The anomalous T_s pattern persists into summer and impacts the precipitation in East Asia by inducing anomalous anti-cyclone at

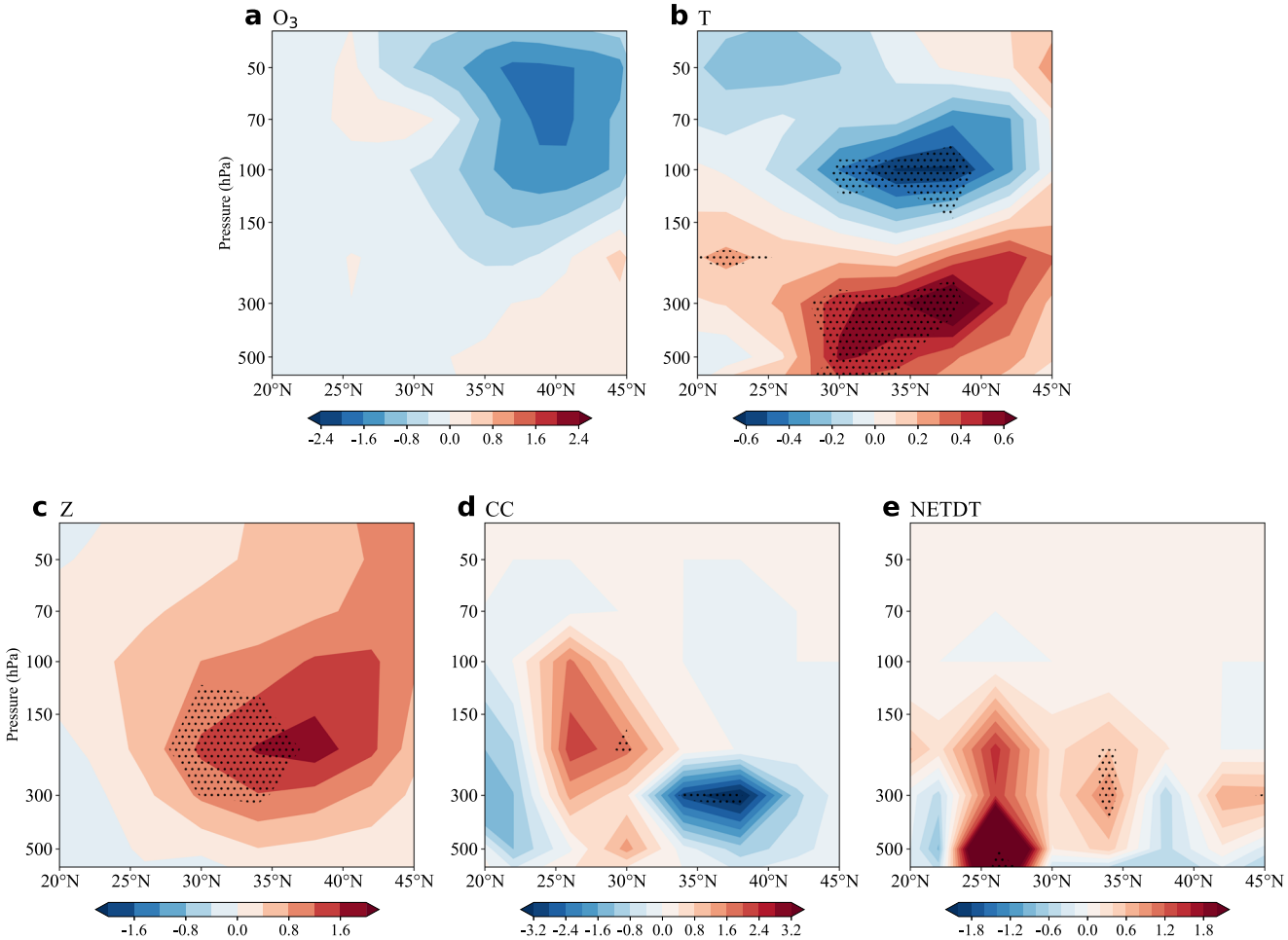

Fig. 7 Vertical-latitude cross sections of OVTP-induced anomalies in MJJ. Vertical-latitude cross-section of **a** ozone mixing ratio (shading, unit: 10^{-7} mol mol^{-1}), **b** temperature (shading, unit: K), **c** geopotential height (shading, unit: gpm), **d** cloud cover (shading, unit: %) and **e** net heating rate (shading, unit: 10^6 K s^{-1}) difference between two experiments (before_remove−after_remove) along 80–105°E. The dotted areas exceed the 90% confidence level.

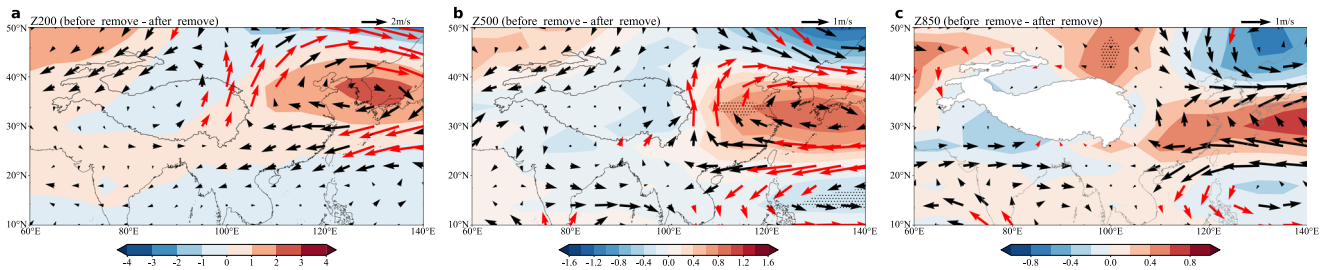

Fig. 8 OVTP-induced atmospheric circulation anomalies in JJA. JJA geopotential height difference (shading, unit: gpm) and wind difference (vector, unit: m s^{-1}) at **a** 850 hPa, **b** 500 hPa, and **c** 850 hPa between two experiments (before_remove−after_remove). The dotted areas and red arrows exceed the 90% confidence level.

850 hPa centered over the Yangtze-Huaihe River Basin, accompanied by easterly wind anomalies along the southeastern coast of China. The anomalous anti-cyclone causes negative precipitation anomalies along the Yangtze River Basin, while the easterly wind anomalies facilitate moisture transport and lead to positive precipitation anomalies in Southern China.

Zhang et al. (2022) evaluated the OVTP in Coupled Model Intercomparison Project Phase 6 (CMIP6) Models and found that the seasonal cycles and spatial characteristics of the OVTP are generally well captured by most models[43]. To demonstrate the significance of the OVTP to East Asian precipitation, we have selected six models participated in CMIP6 (MRI-ESM2-0, GISS-E2-2-G, IPSL-CM5A2-1NCA, MIROC-ES2H, GISS-E2-1-H and MPI-ESM-1-2-HAM)[55–60], each of which includes data on TCO, precipitation, and T_s as the physical variables. Among these models, there are notable differences in capturing the relationship between MJJ OVTPI and JJA TP T_s. Supplementary Table 2 provides information about the models and arranges the correlation coefficients between MJJ OVTP and JJA TP T_s for each model in decreasing order. Given the observational data indicating a robust positive correlation (correlation coefficient of 0.8) between MJJ OVTP and JJA T_s over the TP, most models' performance in simulating this

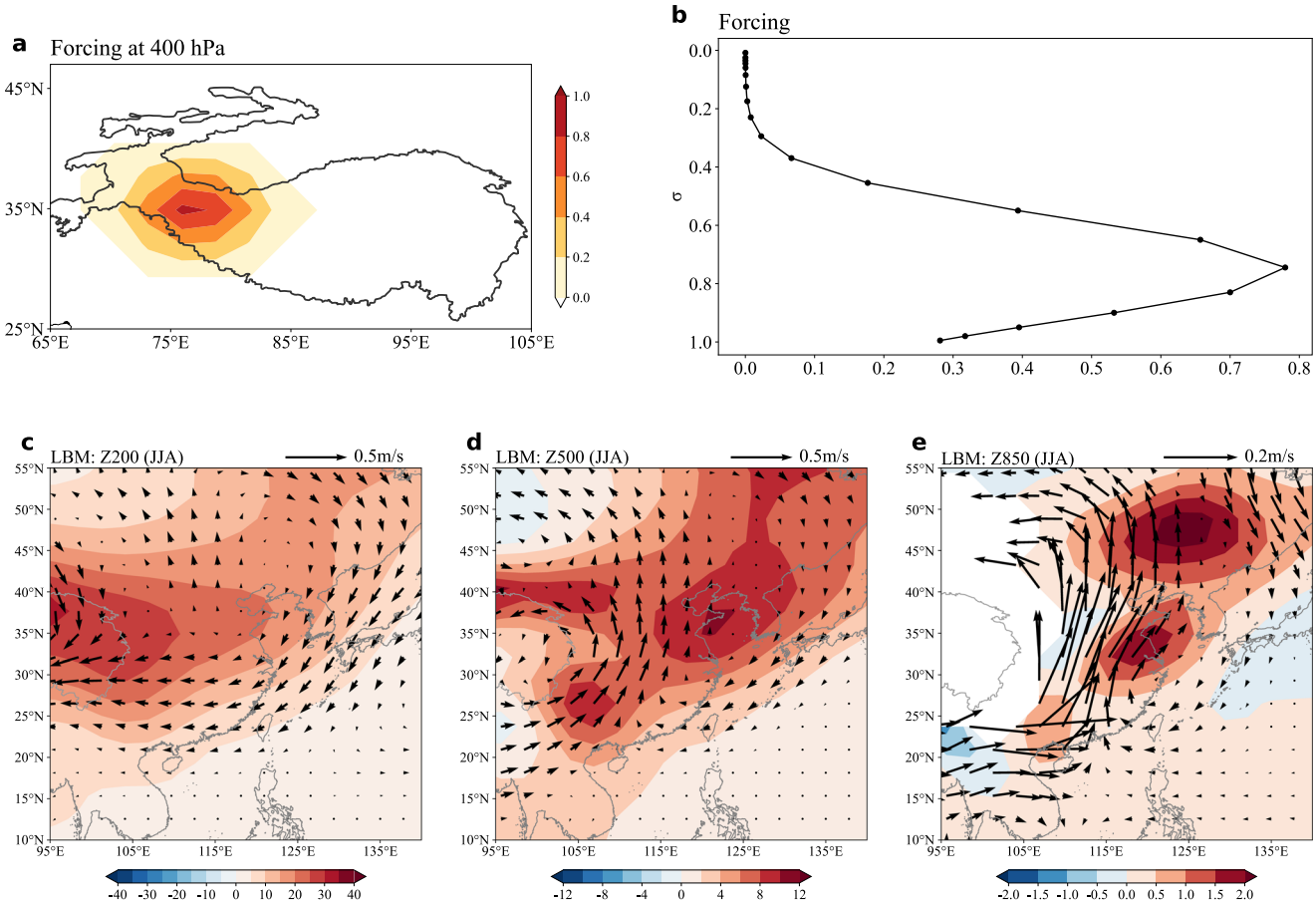

Fig. 9 Atmospheric response to an idealized heating forcing over TP. a The spatial pattern of the heating forcing (shading, unit: K day^{-1}) at the sigma level of 0.75 and **b** the vertical profile of the heating forcing (black curve, unit: K day^{-1}) around the horizontal maximum heating centre (35°N, 77°E). Simulated response of geopotential height (shading, unit: gpm) and wind (vector, unit: m s^{-1}) at **c** 200, **d** 500, **e** 850 hPa to the heating forcing added to the climatological summer atmospheric circulation.

relationship (with a maximum correlation of 0.5 in Supplementary Table 2) requires improvement. Among these models, MRI-ESM2-0 shows the closest simulated correlation coefficient to the observation result (0.8), with a value of 0.5. Meanwhile, this model successfully reproduces the negative precipitation anomalies along the Yangtze River Basin (MRI-ESM2-0 in Fig. 10). However, it does not accurately simulate the positive precipitation anomalies observed in the Indochina Peninsula and Southern China region. As the correlation coefficient between OVTP and T_s declines, the models' ability to capture the modes of East Asian precipitation diminishes. In the lower row of Fig. 10, MIROC-ES2H and GISS-E2-1-H both exhibit positive precipitation anomalies in the Yangtze-Huaihe River Basin, contradicting the observation result. It is crucial to enhance the capability of models to simulate the impacts of OVTP on TP T_s, which, in turn, would improve their ability to simulate the effect of OVTP on East Asian precipitation. Given the projections of deepening OVTP in the future as indicated by most CMIP6 models[43], the significance of the OVTP in impacting East Asian precipitation is expected to become increasingly critical in the coming decades.

METHODS

Reanalysis datasets

The datasets applied in this work include: (1) 1979–2022 monthly TCO, temperature, geopotential height, BLH, TCC, ISHF, horizontal and vertical wind components gridded at 0.25° × 0.25° resolution, available from the European Centre for ECMWF ERA5 reanalysis[61]. (2) 1979–2022 monthly precipitation data acquired from the PRECipitation REConstruction over Ocean (PREC-O) with 2.5° × 2.5° grid[62].

Methodology

In this study, statistical methods such as linear regression analysis and correlated coefficient analysis are employed. The statistical significance test is based on a two-tailed Student's *t*-test.

To assess the impacts of OVTP, we employ the Whole Atmosphere Community Climate Model (WACCM) in this study. The model is derived from the National Center for Atmospheric Research (NCAR) Community Earth System Model version 1.2 (CESM1.2). The Specified-Chemistry version of this model (SC-WACCM) is utilized, which has horizontal resolution of 1.9° × 2.5° and 66 levels in the vertical domain from the ground to 4.5 × 10^{-6} hPa. SC-WACCM is coupled to land, ocean, and sea ice components, allowing for a comprehensive representation of Earth's climate system. This model is designed to operate with prescribed ozone concentrations[63], allowing us to control the initial ozone concentrations and investigate the resulting climate impacts. Furthermore, this model has been widely employed in previous studies to investigate the impact of Antarctic ozone and the ozone layer[64,65]. Therefore, SC-WACCM is well-suited for addressing the objectives of this paper.

To investigate the linear response of the circulation anomaly over East Asia to the TP diabatic heating anomaly, numerical experiments are conducted using the LBM model. The model is developed based on the dynamical core of the Atmospheric

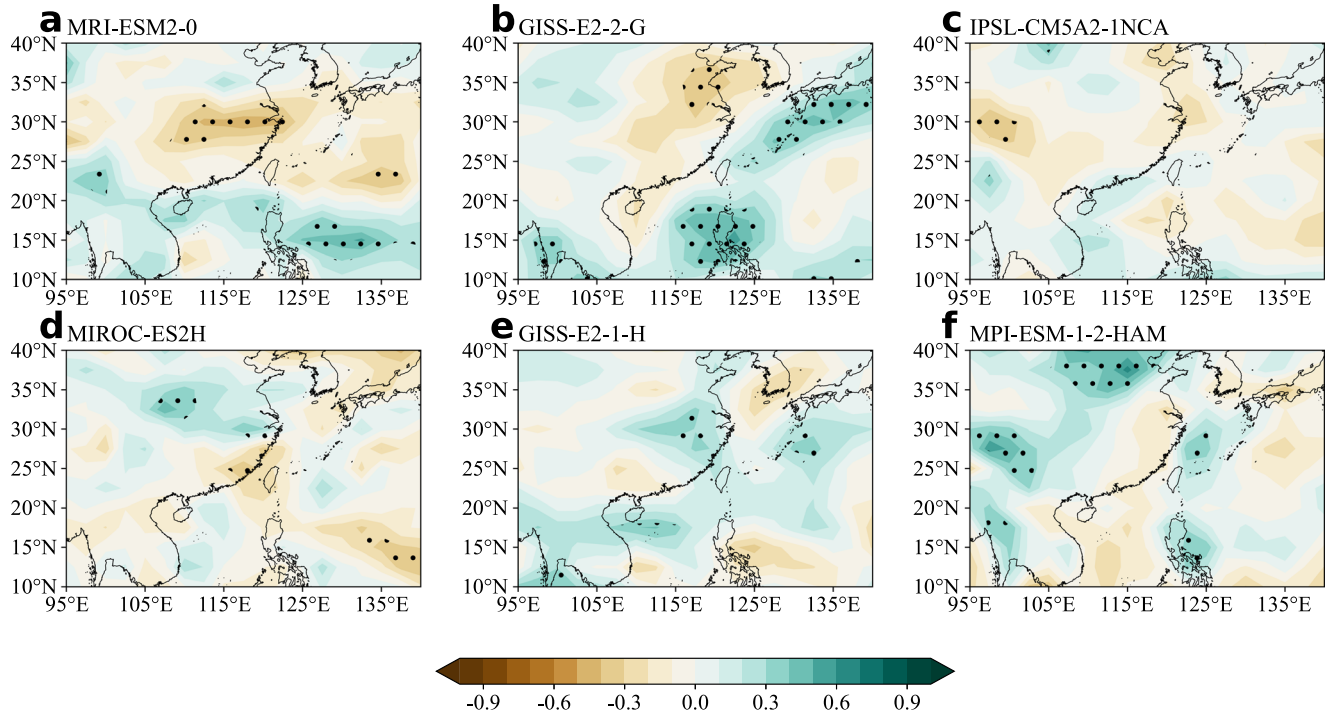

Fig. 10 Relationship between MJJ OVTP and JJA precipitation in CMIP6 models during 1979–2014. The shading represents correlation coefficients between MJJ OVTPI and JJA precipitation for **a** MRI-ESM2-0, **b** GISS-E2-2-G, **c** IPSL-CM5A2-1NCA, **d** MIROC-ES2H, **e** GISS-E2-1-H and **f** MPI-ESM-1-2-HAM. The dotted areas exceed the 90% confidence level.

General Circulation Model (AGCM) and is designed by the Center for Climate System Research at the University of Tokyo and the National Institute for Environmental Studies in Japan[66]. We utilize the dry version of the model with a horizontal resolution of T42 and 20 vertical sigma levels. To obtain a stable atmospheric response to the prescribed thermal forcing, we employ the time integration method, which has been widely used in previous studies[67,68].

In this study, an OVTP index (OVTPI) is determined by the inverse zonal deviation of TCO averaged within the TP domain (75°−90°E, 32.5°−42.5°N). Specifically, a higher OVTPI value indicates a stronger OVTP.

DATA AVAILABILITY

The ERA5 data are available from the European Centre for Medium-Range Weather Forecasts (ECMWF) website (https://www.ecmwf.int/en/forecasts/dataset/ecmwf-reanalysis-v5). The PREC-O data are obtained from the NOAA website (https://psl.noaa.gov/data). The CMIP6 models can be downloaded from https://esgf-node.llnl.gov/search/cmip6/. The experiment datasets used in this study are available from the first author upon reasonable request.

CODE AVAILABILITY

All figures in this paper are produced by Python version 3.7.9, and the source codes can be obtained upon request to the first author.

Received: 15 June 2023; Accepted: 23 October 2023;
Published online: 01 November 2023

REFERENCES

1. Bais, A. et al. Ozone depletion and climate change: impacts on UV radiation. *Photochem. Photobiol. Sci.* **14**, 19–52 (2015).
2. Ramanathan, V. & Dickinson, R. The role of stratospheric ozone in the zonal and seasonal radiative energy balance of the earth-troposphere system. *J. Atmos. Sci.* **36**, 1084–1104 (1979).
3. Polvani, L., Waugh, D., Correa, G. & Son, S. Stratospheric ozone depletion: the main driver of twentieth-century atmospheric circulation changes in the Southern Hemisphere. *J. Clim.* **24**, 795–812 (2011).
4. Son, S. et al. Impact of stratospheric ozone on Southern Hemisphere circulation change: a multimodel assessment. *J. Geophys. Res.* **115**, https://doi.org/10.1029/2010JD014271 (2010).
5. Shepherd, T. et al. Separating the dynamical effects of climate change and ozone depletion. Part II: Southern Hemisphere troposphere. *J. Clim.* **24**, 1850–1868 (2011).
6. Son, S. et al. The impact of stratospheric ozone recovery on the Southern Hemisphere westerly jet. *Science* **320**, 1486–1489 (2008).
7. Son, S., Tandon, N., Polvani, L. & Waugh, D. Ozone hole and Southern Hemisphere climate change. *Geophys. Res. Lett.* **36**, https://doi.org/10.1029/2009GL038671 (2009).
8. Kang, S., Polvani, L., Fyfe, J. & Sigmond, M. Impact of polar ozone depletion on subtropical precipitation. *Science* **332**, 951–954 (2011).
9. Karpechko, A., Perlwitz, J. & Manzini, E. A model study of tropospheric impacts of the Arctic ozone depletion 2011. *J. Geophys. Res. Atmos.* **119**, 7999–8014 (2014).
10. Calvo, N., Polvani, L. & Solomon, S. On the surface impact of Arctic stratospheric ozone extremes. *Environ. Res. Lett.* **10**, https://doi.org/10.1088/1748-9326/10/9/094003 (2015).
11. Ivy, D., Solomon, S., Calvo, N. & Thompson, D. Observed connections of Arctic stratospheric ozone extremes to Northern Hemisphere surface climate. *Environ. Res. Lett.* **12**, https://doi.org/10.1088/1748-9326/aa57a4 (2017).
12. Sigmond, M. & Fyfe, J. Has the ozone hole contributed to increased Antarctic sea ice extent? *Geophys. Res. Lett.* **37**, https://doi.org/10.1029/2010GL044301 (2010).
13. Xia, Y. et al. Stratospheric ozone-induced cloud radiative effects on Antarctic Sea Ice. *Adv. Atmos. Sci.* **37**, 505–514 (2020).
14. Zhang, J. et al. Responses of Arctic sea ice to stratospheric ozone depletion. *Sci. Bull. (Beijing)* **67**, 1182–1190 (2022).
15. Turner, J. et al. Non-annular atmospheric circulation change induced by stratospheric ozone depletion and its role in the recent increase of Antarctic sea ice extent. *Geophys. Res. Lett.* **36**, https://doi.org/10.1029/2009GL037524 (2009).
16. Bitz, C. & Polvani, L. Antarctic climate response to stratospheric ozone depletion in a fine resolution ocean climate model. *Geophys. Res. Lett.* **39**, https://doi.org/10.1029/2012GL053393 (2012).

17. Hall, A. & Visbeck, M. Synchronous variability in the Southern Hemisphere atmosphere, sea ice, and ocean resulting from the annular mode. *J. Clim.* **15**, 3043–3057 (2002).
18. Zhou, X. & Luo, C. Ozone valley over Tibetan plateau. *Acta Meteorol. Sin.* **8**, 505–506 (1994).
19. Zheng, X. et al. Observation study on Total Ozone Amount and its vertical profile over Lhasa in the summer of 1998. *J. Appl. Meteorol. Sci.* **11**, 173–179 (2000).
20. Guo, D., Su, Y., Shi, C., Xu, J. & Powell, A. M. Double core of ozone valley over the Tibetan Plateau and its possible mechanisms. *J. Atmos. Sol.-Terr. Phys.* **130–131**, 127–131 (2015).
21. Guo, F. et al. Effects of nitrogen oxides produced from lightning on the formation of the Ozone Valley over the Tibetan Plateau. *Chin. J. Atmos. Sci.* **43**, 266–276 (2019).
22. Fu, C., Li, W. L. & Zhou, X. J. *Ozone Changs and Effects on Climate and Environment in China*, *Part 2* (in Chinese) (China Meteorological Press, Beijing, 1997).
23. Liu, Y., Li, W., Zhou, X. & He, J. Mechanism of formation of the ozone valley over the Tibetan Plateau in summer—transport and chemical process of ozone. *Adv. Atmos. Sci.* **20**, 103–109 (2003).
24. Tian, W., Chipperfield, M. & Huang, Q. Effects of the Tibetan Plateau on total column ozone distribution. *Tellus B Chem. Phys. Meteorol.* **60**, 622–635 (2008).
25. Bian, J., Yan, R., Chen, H., Lü, D. & Massie, S. Formation of the summertime ozone valley over the Tibetan Plateau: the Asian summer monsoon and air column variations. *Adv. Atmos. Sci.* **28**, 1318–1325 (2011).
26. Ye, Z. & Xu, Y. Climate characteristics of ozone over Tibetan Plateau. *J. Geophys. Res. Atmos.* **108**, https://doi.org/10.1029/2002JD003139 (2003).
27. Bian, J. et al. Ozone mini-hole occurring over the Tibetan Plateau in December 2003. *Chin. Sci. Bull.* **51**, 885–888 (2006).
28. Bian, J. et al. Transport of Asian surface pollutants to the global stratosphere from the Tibetan Plateau region during the Asian summer monsoon. *Natl Sci. Rev.* **7**, 516–533 (2020).
29. Cong, C., Li, W. & Zhou, X. Mass exchange between stratosphere and troposphere over the Tibetan Plateau and its surroundings. *Chin. Sci. Bull.* **47**, 508–512 (2002).
30. Fan, W. et al. The distribution of cross-tropopause mass flux over the Tibetan Plateau and its surrounding regions. *Chin. J. Atmos. Sci.* **32**, 1309–1318 (2008).
31. Zhou, S. & Zhang, R. Decadal variations of temperature and geopotential height over the Tibetan Plateau and their relations with Tibet ozone depletion. *Geophys. Res. Lett.* **32**, https://doi.org/10.1029/2005GL023496 (2005).
32. Guo, D., Wang, P., Zhou, X., Liu, Y. & Li, W. Dynamic effects of the South Asian high on the ozone valley over the Tibetan Plateau. *Acta Meteorol. Sin.* **26**, 216–228 (2012).
33. Li, Y. et al. Analysis and attribution of total column ozone changes over the Tibetan Plateau during 1979–2017. *Atmos. Chem. Phys.* **20**, 8627–8639 (2020).
34. Zhang, J. et al. Climate warming and decreasing total column ozone over the Tibetan Plateau during winter and spring. *Tellus B Chem. Phys. Meteorol.* **66**, https://doi.org/10.3402/tellusb.v66.23415 (2014).
35. Li, Z. et al. Impact of ozone valley over the Tibetan Plateau on the South Asian High in CAM5. *Adv. Meteorol.* **2017**, 1–8 (2017).
36. Qin, H. et al. The Interaction between variations of South Asia High and Ozone in the adjacent regions. *Chin. J. Atmos. Sci.* **42**, 421–434 (2018).
37. Zhou, R. & Chen, Y. Effects of variation of low ozone center over the Tibetan Plateau on climate in China. *Chin. J. Atmos. Sci.* **31**, https://doi.org/10.3878/j.issn.1006-9895.2007.03.11 (2007).
38. Zha, P. & Wu, Z. Contribution of the Tibetan Plateau winter snow cover to seasonal prediction of the East Asian summer monsoon. *Atmos. Ocean.* **61**, 25–39 (2023).
39. Xiao, Z. & Duan, A. Impacts of Tibetan Plateau snow cover on the interannual variability of the East Asian summer monsoon. *J. Clim.* **29**, 8495–8514 (2016).
40. Jin, R., Wu, Z. & Zhang, P. Tibetan Plateau capacitor effect during the summer preceding ENSO: from the Yellow River climate perspective. *Clim. Dyn.* **51**, 57–71 (2018).
41. Qian, Y., Zhang, Y., Huang, Y., Huang, Y. & Yao, Y. The effects of the thermal anomalies over the Tibetan Plateau and its vicinities on climate variability in China. *Adv. Atmos. Sci.* **21**, 369–381 (2004).
42. Zhao, P., Yang, S. & Yu, R. Long-term changes in rainfall over eastern China and large-scale atmospheric circulation associated with recent global warming. *J. Clim.* **23**, 1544–1562 (2010).
43. Zhang, K. et al. Evaluating the ozone valley over the Tibetan Plateau in CMIP6 models. *Adv. Atmos. Sci.* **39**, 1167–1183 (2021).
44. Zhou, L., Zou, H., Ma, S. & Li, P. The Tibetan ozone low and its long-term variation during 1979–2010. *Acta Meteorol. Sin.* **27**, 75–86 (2013).
45. Ramaswamy, V., Schwarzkopf, M. & Randel, W. Fingerprint of ozone depletion in the spatial and temporal pattern of recent lower-stratospheric cooling. *Nature* **382**, 616–618 (1996).
46. Bengtsson, L., Roeckner, E. & Stendel, M. Why is the global warming proceeding much slower than expected? *J. Geophys. Res. Atmos.* **104**, 3865–3876 (1999).
47. Hu, D., Tian, W., Xie, F., Wang, C. & Zhang, J. Impacts of stratospheric ozone depletion and recovery on wave propagation in the boreal winter stratosphere. *J. Geophys. Res. Atmos.* **120**, 8299–8317 (2015).
48. Wu, Z., Jiang, Z., Li, J., Zhong, S. & Wang, L. Possible association of the western Tibetan Plateau snow cover with the decadal to interdecadal variations of northern China heatwave frequency. *Clim. Dyn.* **39**, 2393–2402 (2012).
49. Wu, Z., Zhang, P., Chen, H. & Li, Y. Can the Tibetan Plateau snow cover influence the interannual variations of Eurasian heat wave frequency? *Clim. Dyn.* **46**, 3405–3417 (2015).
50. Alexander, L. Extreme heat rooted in dry soils. *Nat. Geosci.* **4**, 12–13 (2011).
51. Hirschi, M. et al. Observational evidence for soil-moisture impact on hot extremes in southeastern Europe. *Nat. Geosci.* **4**, 17–21 (2011).
52. Liu, Y., Xue, Y., Li, Q., Lettenmaier, D. & Zhao, P. Investigation of the variability of near-surface temperature anomaly and its causes over the Tibetan Plateau. *J. Geophys. Res. Atmos.* **125**, https://doi.org/10.1029/2020JD032800 (2020).
53. Qiu, Y., Feng, J., Wang, J., Xue, Y. & Xu, Z. Memory of land surface and subsurface temperature (LST/SUBT) initial anomalies over Tibetan Plateau in different land models. *Clim. Dyn.* 1–16, https://doi.org/10.1007/s00382-021-05937-z (2021).
54. Pan, L. Observed positive feedback between the NAO and the North Atlantic SSTA tripole. *Geophys. Res. Lett.* **32**, https://doi.org/10.1029/2005GL022427 (2005).
55. Sepulchre, P. et al. IPSL-CM5A2—an Earth system model designed for multi-millennial climate simulations. *Geosci. Model Dev.* **13**, 3011–3053 (2020).
56. NASA Goddard Institute for Space Studies (NASA/GISS). *NASA-GISS GISS-E2-2-G Model Output Prepared for CMIP6 CMIP amip. Version 20230904*. Earth System Grid Federation. https://doi.org/10.22033/ESGF/CMIP6.6986 (2019).
57. NASA Goddard Institute for Space Studies (NASA/GISS). *NASA-GISS GISS-E2.1H Model Output Prepared for CMIP6 CMIP. Version 20230904*. Earth System Grid Federation. https://doi.org/10.22033/ESGF/CMIP6.1421 (2018).
58. Watanabe, S. et al. *MIROC MIROC-ES2H Model Output Prepared for CMIP6 GeoMIP. Version 20230904*. Earth System Grid Federation. https://doi.org/10.22033/ESGF/CMIP6.907 (2021).
59. Yukimoto, S. et al. *MRI MRI-ESM2.0 Model Output Prepared for CMIP6 CMIP. Version 20230904*. Earth System Grid Federation. https://doi.org/10.22033/ESGF/CMIP6.621 (2019).
60. Neubauer, D. et al. *HAMMOZ-Consortium MPI-ESM1.2-HAM Model Output Prepared for CMIP6 CMIP Historical. Version 20230904*. Earth System Grid Federation https://doi.org/10.22033/ESGF/CMIP6.5016 (2019).
61. Hersbach, H. et al. *Era5 Monthly Averaged Data on Pressure Levels from 1979 to Present*. Copernicus Climate Change Service (C3S) Climate Data Store (CDS) (2019).
62. Chen, M., Xie, P., Janowiak, J. & Arkin, P. Global land precipitation: a 50-yr monthly analysis based on gauge observations. *J. Hydrol.* **3**, 249–266 (2002).
63. Smith, K. & Polvani, L. The surface impacts of Arctic stratospheric ozone anomalies. *Environ. Res. Lett.* **9**, https://doi.org/10.1088/1748-9326/9/7/074015 (2014).
64. Chiodo, G. & Polvani, L. The response of the ozone layer to quadrupled CO2 concentrations: implications for climate. *J. Clim.* **32**, 7629–7642 (2019).
65. Xia, Y., Xu, W., Hu, Y. & Xie, F. Southern-Hemisphere high-latitude stratospheric warming revisit. *Clim. Dyn.* **54**, 1671–1682 (2020).
66. Watanabe, M. & Kimoto, M. Atmosphere–ocean thermal coupling in the North Atlantic: a positive feedback. *Q. J. R. Meteorol. Soc.* **126**, 3343–3369 (2000).
67. Cao, C. & Wu, Z. Modulation of the Tibetan Plateau snow cover on the interannual variations of the MJO-related winter surface air temperature anomalies over East Asia. *Clim. Dyn.* **59**, 3427–3437 (2022).
68. Zhong, W. & Wu, Z. Subseasonal strength reversal of the East Asian winter monsoon. *Clim. Dyn.* **61**, 709–727 (2023).

ACKNOWLEDGEMENTS

This research was jointly supported by the Second Tibetan Plateau Scientific Expedition and Research (STEP) program (Grant No. 2019QZKK0102), National Natural Science Foundation of China (NSFC) Major Research Plan on West-Pacific Earth System Multi-spheric Interactions (project number: 92158203) and NSFC (Grant No. 91937302).

AUTHOR CONTRIBUTIONS

L.Z. and Z.W. designed the study. The data collection, data analysis and model designments were performed by L.Z. The first draft of the manuscript was written by L.Z. and all authors reviewed the manuscript.

COMPETING INTERESTS

The authors declare no competing interests.

ADDITIONAL INFORMATION

Supplementary information The online version contains supplementary material available at https://doi.org/10.1038/s41612-023-00508-x.

Correspondence and requests for materials should be addressed to Zhiwei Wu.

Reprints and permission information is available at http://www.nature.com/reprints

Publisher's note Springer Nature remains neutral with regard to jurisdictional claims in published maps and institutional affiliations.